

Optics Letters

Uniqueness in multispectral constant-wave epi-illumination imaging

P. B. GARCIA-ALLENDE,¹ K. RADRICH,¹ P. SYMVOULIDIS,¹ J. GLATZ,¹ M. KOCH,¹ K. M. JENTOFT,¹ J. RIPOLL,² AND V. NTZIACHRISTOS^{1,*}

¹Chair for Biological Imaging & Institute for Biological and Medical Imaging, Technische Universität München and Helmholtz Zentrum München, Trogerstr. 9 D-81675 München, Germany

²Department of Bioengineering and Aerospace Engineering, University Carlos III of Madrid, Avda. de la Universidad 30, 28911 Madrid, Spain

*Corresponding author: v.ntziachristos@tum.de

Received 29 April 2016; revised 1 June 2016; accepted 2 June 2016; posted 7 June 2016 (Doc. ID 261583); published 29 June 2016

Multispectral tissue imaging based on optical cameras and continuous-wave tissue illumination is commonly used in medicine and biology. Surprisingly, there is a characteristic absence of a critical look at the quantities that can be uniquely characterized from optically diffuse matter by multispectral imaging. Here, we investigate the fundamental question of uniqueness in epi-illumination measurements from turbid media obtained at multiple wavelengths. By utilizing an analytical model, tissue-mimicking phantoms, and an *in vivo* imaging experiment we show that independent of the bands employed, spectral measurements cannot uniquely retrieve absorption and scattering coefficients. We also establish that it is, nevertheless, possible to uniquely quantify oxygen saturation and the Mie scattering power—a previously undocumented uniqueness condition. © 2016 Optical Society of America

OCIS codes: (170.0110) Imaging systems; (170.1470) Blood or tissue constituent monitoring; (170.1610) Clinical applications; (170.3660) Light propagation in tissues; (170.3880) Medical and biological imaging; (170.4580) Optical diagnostics for medicine.

<http://dx.doi.org/10.1364/OL.41.003098>

Epi-illumination tissue imaging using optical cameras is commonly employed in diagnostic and theranostic medicine, for example, in surgery, endoscopy, or dermatology [1–3]. While conventional color imaging is performed at three or four spectral bands, imaging at an increased number of wavelengths, dubbed multispectral, has been considered for improving the diagnostic value of these procedures [4]. In dermatology, multispectral epi-illumination imaging has been investigated for melanoma diagnoses [5] or for assessing the burn depth and the healing timeline [6] and in ophthalmology for detecting retinal diseases and estimating oximetry maps [7]. Likewise, endoscopic narrow band imaging (NBI) utilizes a blue and a green spectral band to highlight subsurface blood vessels and enhance the diagnostic yield of white-light endoscopy [8].

The larger part of diagnostic optical imaging is based on the qualitative observation of images or empirical processing. Disease is detected, for example, by color deviation from the appearance of healthy tissue. Quantification of tissue optical properties is a sought-after target for improving the detection ability and elucidating underlying pathophysiological features [9,10]. In particular, quantification of tissue absorption or scattering changes may lead to improved diagnostics [11]. The majority of clinical optical imaging is based on measurements performed under constant intensity illumination, i.e., continuous wave (CW). However, CW measurements are not capable of retrieving tissue absorption and scattering. In particular, it is known [3] that the optical intensity reflected from a diffusive surface at a single wavelength depends on the quotient between the reduced scattering (μ'_s) and the absorption (μ_a) coefficient at the respective wavelength—a condition referred to as “scale invariance” [3,12]. While the inability of single wavelength CW epi-illumination measurements to quantify tissue properties is established, that of measurements obtained at multiple wavelengths has not yet been analytically demonstrated. To the best of our knowledge, no investigation has examined uniqueness in the context of multispectral measurements. The underlying premise of this interrogation relates to whether the information carried by apparently independent measurements at different wavelengths indeed conveys independent information. We therefore addressed the fundamental question on whether there exist tissue parameters that can be uniquely quantified by epi-illumination measurements at multiple wavelengths. This study of uniqueness was initially based on a theoretical analysis and then confirmed experimentally.

To study the uniqueness achieved by multispectral epi-illumination measurements, we use an analytical expression describing epi-illumination measurements [13]. We have recently validated [14] this newly proposed reflectance model that accounts for the exponential decay of the reduced intensity as it enters the diffusive medium [15]. Assuming a detector having a numerical aperture of 1, a turbid medium of index of refraction n_0 and plane-wave CW illumination, the light flux detected at the interface is given by [13]

$$J_{\text{det}} = \frac{S_0 \mu'_s \sqrt{D \mu_a}}{((\mu'_s + \mu_a) \sqrt{D \mu_a} + \mu_a) (1 + \alpha \sqrt{D \mu_a})}, \quad (1)$$

where $S_0 = (1 - R_{\text{air} \rightarrow n_0}) S^{\text{inc}}$ is the power per area that enters the diffusive medium (in $\text{W} \cdot \text{cm}^{-2}$). S_0 incorporates the power lost due to specular reflections with respect to the total incident power per area S^{inc} ; μ_a and μ'_s are, respectively, the absorption and reduced scattering coefficient of the turbid medium; and $D = 1/3(\mu'_s + \beta \mu_a)$ is the absorption-dependent diffusion coefficient, whereby β indicates the D dependence on absorption and typically ranges from 0.2 to 0.5 [16]. Note that this dependence with absorption is nonlinear since the factor β is also absorption and scattering dependent. This nonlinear dependence of the diffusion coefficient with absorption could, in principle, enable the separation of absorption from scattering. However, as demonstrated subsequently, the coefficient β further depends on the quotient of μ'_s and μ_a , not relaxing the nonunique characteristic of wavelength-dependent separation of μ'_s and μ_a . Finally, in Eq. (1), the boundary coefficient α accounts for the difference in refractive indices [17]. Introducing the expression for the diffusion coefficient in Eq. (1) and dividing the numerator and denominator by μ'_s , the detected flux becomes

$$J_{\text{det}} = \frac{(1 - R_{\text{air} \rightarrow n_0}) S^{\text{inc}} \sqrt{\frac{1}{3(\bar{\mu} + \beta)}}}{\left(\left(1 + \frac{1}{\bar{\mu}}\right) \sqrt{\frac{1}{3(\bar{\mu} + \beta)}} + \frac{1}{\bar{\mu}} \right) \left(1 + \alpha \sqrt{\frac{1}{3(\bar{\mu} + \beta)}}\right)}, \quad (2)$$

where $\bar{\mu} = \mu'_s / \mu_a$. The factor β remains dependent on μ'_s and μ_a . One would assume that under certain conditions, such as the presence of high absorption, the absorption dependence of the diffusion coefficient would provide a means to reduce the scale invariance of J_{det} . However, in order to analyze the scale invariance of J_{det} with $\bar{\mu}$, we first need to prove the invariance of β with respect to μ'_s and μ_a . This analysis provides the formal mathematical proof for the scale invariance on $\bar{\mu}$ assumed in [3]. According to Aronson *et al.* [16], this dependence of β on the optical properties is given by

$$\begin{aligned} \beta &= \frac{1}{3D\mu_a} - \frac{\mu'_s}{\mu_a} = \frac{1}{3\frac{\mu_a^2}{F_n \mu'_s}} - \frac{\mu'_s}{\mu_a} = \frac{1}{3\frac{\mu_a^2}{F_n(\mu_a + \frac{\mu'_s}{1-g})}} - \frac{\mu'_s}{\mu_a} \\ &= \frac{F_n(\mu_a + \frac{\mu'_s}{1-g})^2}{3\mu_a^2} - \frac{\mu'_s}{\mu_a} = \frac{1}{3} F_n \left(1 + \frac{\bar{\mu}}{1-g}\right) - \bar{\mu} \\ F_n &= b_0 b_1 \left[1 - \frac{4b_0}{b_2} + \left(\frac{4b_0}{b_2}\right)^2 \left(1 - \frac{9b_1}{4b_3}\right) - \left(\frac{4b_0}{b_2}\right)^3 \right. \\ &\quad \left. \times \left(1 - \frac{27b_1}{4b_3} + \frac{81b_1^2}{16b_3^2} + 9\frac{b_1^2 b_2}{b_3^2 b_4}\right) + \dots \right], \quad (3) \end{aligned}$$

where $b_1 = (2l + 1)(1 - \omega g^l)$, with l being the index of the infinite series. Since $\omega = \mu_s / \mu_t$, it is possible to rewrite each term in Eq. (3) in terms of the quotient between the reduced scattering coefficient and the absorption coefficient ($\bar{\mu}$) and the anisotropy parameter (g) as

$$b_1 = (2l + 1) \left(1 - \frac{\bar{\mu}}{1-g + \bar{\mu} g^l}\right). \quad (4)$$

Equation (4) demonstrates that in spite of including the coefficient β in the analysis, the scale invariance on $\bar{\mu}$ holds for the single wavelength case since $\beta(\mu'_s, \mu_a) = \beta(\bar{\mu})$. Figure 1 plots the

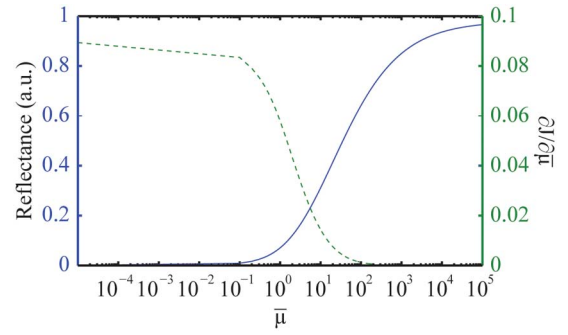


Fig. 1. Dependence of the reflectance (solid line) and the derivative of the reflectance (dotted line) on the quotient of the reduced scattering and absorption coefficient ($\bar{\mu}$).

reflectance or the light flux normalized to the incident flux S_0 as a function of $\bar{\mu}$, where it can be seen that J_{det}/S_0 is an injective function, i.e., it monotonically increases with $\bar{\mu}$ and its derivative is always positive and distinct from zero. Therefore, one and only one value of the reflectance corresponds to one value of the quotient between the reduced scattering and the absorption coefficient, and the reflectance function is invertible for $\bar{\mu}$.

Assuming blood is the sole absorber, we may now introduce in the expression for $\bar{\mu}$ the spectral properties of the tissue chromophores and the Mie scattering factors:

$$\mu_a(\lambda) = c_{\text{blood}} [\text{StO}_2 \mu_a^{\text{HbO}_2}(\lambda) + (1 - \text{StO}_2) \mu_a^{\text{Hb}}(\lambda)] \quad (5)$$

$$\mu'_s(\lambda) = A \lambda^{-b}, \quad (6)$$

where c_{blood} corresponds to the blood volume fraction, StO_2 is the oxygen saturation, $\mu_a^{\text{HbO}_2}(\lambda)$ and $\mu_a^{\text{Hb}}(\lambda)$ are, respectively, the absorption coefficients of oxygenated and de-oxygenated blood, and A and b are the scattering amplitude and the scattering power of the power law dependence on wavelength used to describe the Mie scattering spectrum, respectively. The oxygen saturation and the scattering power can be extracted from at least three multispectral measurements, but it is not possible to decouple the scattering amplitude and the absolute blood concentration:

$$\bar{\mu}(\lambda) = \frac{\mu'_s(\lambda)}{\mu_a(\lambda)} = \frac{A \lambda^{-b}}{c_{\text{blood}} [\text{StO}_2 \mu_a^{\text{HbO}_2}(\lambda) + (1 + \text{StO}_2) \mu_a^{\text{Hb}}(\lambda)]}. \quad (7)$$

This implies that given a semi-infinite homogenous turbid medium with specific blood concentration c_{blood} and scattering amplitude A_1 , the normalized diffuse reflectance for every wavelength from any other turbid medium with the same oxygen saturation and scattering power and matching the conditions $c_{\text{blood}_2}/c_{\text{blood}_1} = A_2/A_1$ will be identical. This coupling of the absolute optical properties results from the extension of the “scale invariance” condition stated above for a single wavelength to the multispectral case.

In order to confirm the theoretical predictions of Eqs. (2) and (7) and to estimate the overall accuracy in predicting the oxygen saturation, the scattering power, and the ratio between the blood concentration and the scattering amplitude, we first performed an experiment on homogeneous liquid phantoms of known optical properties. Then a more realistic experiment in

an *in vivo* imaging scenario on a murine model was carried out. Phantoms were composed of Intralipid to mimic scattering and blood diluted in NaCl. Intralipid concentration varied from 0.4% to 2%, being the corresponding reduced scattering coefficients computed with the formulation from Michels *et al.* [18]. Blood concentration varied between 2%, 4%, and 6%. Saturation levels covered the 0–100% range and were obtained adding different amounts of sodium hydrosulfite (Sigma–Aldrich, USA) [19]. A blood gas analyzer was employed to measure the ground-truth values. The experimental setup employed has been described elsewhere [14]. An ~ 2 cm \times 2 cm region of interest from each spectral image was selected and divided into 40×40 elements of 25 mm^2 area, and the mean values per element and wavelength were computed. System calibration was obtained by measuring the spectral reflectance from a phantom containing only 0.5% Intralipid used to normalize all other spectral reflectance curves. Normalized curves were fitted to Eq. (2) according to a least-squares-fitting procedure to extract the relevant parameters, being the upper and lower bounds for the optimization fixed to their physiological ranges [20]. The anisotropy parameter g was assumed constant over wavelength and equal to 0.8. Retrieved reduced scattering coefficients were expressed in terms of their relative value with respect to the scattering coefficient of Intralipid 1% at 600 nm [18]. The recovered parameters presented a strong correlation with their true values. The adjusted $R^2 > 0.95$ for $c_{\text{blood}} = A$ and > 0.98 for the oxygenation level, and the root-mean-square errors were 0.041% and 2.1%, respectively. The estimated scattering power varied within the range of $\bar{b} \pm \sigma_b = 1.24 \pm 0.17$ for all test phantoms, which is in good agreement with the assumed scattering power ($b = 1.32$) derived from Michels *et al.* [18].

To further confirm Eq. (7), we imaged the exposed abdomen of an anaesthetized CD1 mouse under regular and 100% O_2 inhalation. The mouse was then sacrificed under anaesthesia. All procedures were approved by the District Government of Upper Bavaria. Acquisition exposure times varied in the 76.2 ms–2.3 s range while interimage intervals were of the order of several hundreds of milliseconds. This gave rise to significant pixel misalignments due to motion artifacts. Consequently, motion correction between consecutive images was performed using the speeded-up robust features (SURF) algorithm [21]. The spectra were corrected on a per-pixel basis using a measurement from a Spectralon block (Ocean Optics, WS1 Reflectance Standard), employed herein as the reflectance standard. Normalized spectra were then fitted to Eq. (7). The results of these measurements are shown in Fig. 2. Color images composed from the multispectral images are shown in the left column, while the subsequent columns depict the corresponding images of oxygen saturation, the ratio between the absolute blood concentration and the scattering concentration, and the scattering power, respectively. As highlighted in the bottom graph, the oxygenation values changed dynamically in relationship to the air mixture inhaled by the mouse and eventually decreased when reaching postmortem. The absolute values differ significantly among organs. These differences have also been observed in oxygenation measurements based on alternative approaches [22], and, as a consequence of the used model, it averages the real oxygen saturations over the probed tissue volumes per location. As expected, the maps of $c_{\text{blood}} = A$ and the scattering power barely changed during the variations in the oxygen

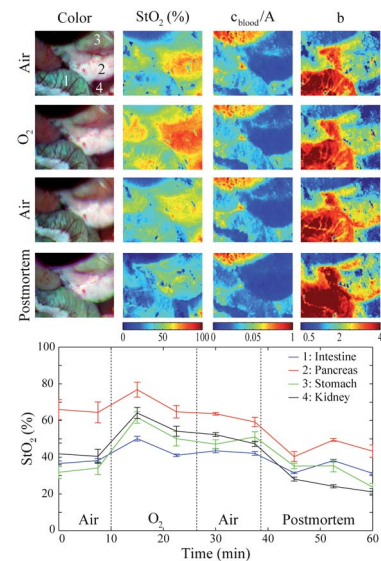


Fig. 2. Emulation of an intraoperative environment in a CD1 mouse. Top images: color images before turning on the oxygen flow, when breathing 100% O_2 and normal air again, and after the mouse was euthanized. The corresponding oxygen saturation, $c_{\text{blood}} = A$, and scattering power images are displayed in the second to fourth columns. Bottom graph: averaged oxygen saturation and standard deviations obtained over regions of interest per organ as a function of time.

saturation values and provide delineation of the different organs. Estimated values of the parameters for the imaged organs are shown in Table 1. The estimated value of the scattering power for the stomach, in particular, is in good agreement with the values reported in the available literature [20], while those of kidney and bowel differ more significantly.

In this Letter, we demonstrated that multispectral measurements of the total diffuse reflectance under constant illumination are scale-invariant with respect to the quotient between absolute values of scattering and blood concentration. To circumvent this limitation, several alternatives have been considered. For oxygen saturation quantification, tissue scattering is commonly assumed to be spatially uniform and known *a priori* [4] or constant with wavelength [23]. These assumptions may lead to significant errors in calculating oxygen saturation maps [24]. To minimize these errors, the differential path length method [25] has also been suggested [24]. The wavelength dependence of the mean path length in tissue is estimated using mostly Monte Carlo simulations, and then the changes in the chromophore concentrations are computed using a modified Beer–Lambert law that incorporates this variable transport path length [26]. The determination of scattering and absorption without the need for assumptions is typically performed by

Table 1. Estimated Values of $c_{\text{blood}} = A$ and b of the Imaged Organs

Organ	$c_{\text{blood}} = A$	b
Intestine	0.031 ± 0.004	3.4 ± 0.3
Pancreas	0.010 ± 0.009	2.2 ± 0.3
Stomach	0.016 ± 0.002	0.8 ± 0.5
Kidney	0.039 ± 0.002	1.1 ± 0.3

multiple measurements of light intensity at different distances away from a point illumination source [3]; however, such approach is not applicable to wide-field camera-based imaging. Alternatively, the use of pulsed- [27], intensity-modulated light [28], or the projection of patterns at multiple spatial frequencies [29] has been suggested. These alternative imaging methods gather additional information to measure scattering concurrently with absorption but at the expense of system cost and complexity. We established herein that, for the determination of tissue oxygenation, it is not necessary to employ more costly and complex alternatives, thus avoiding pitfalls stemming from partial cross talk among optical parameters [30]. Instead, the determination of tissue oxygenation can be based on CW, plane-illumination measurements without making *a priori* assumptions on the scattering tissue properties. In addition, multispectral measurements may also be used to compute the power law dependence on wavelength, which provides tissue morphology information at the microscopic level.

The proposed methodology has been demonstrated in liquid tissue-mimicking phantoms, where strong correlation with the expected values was obtained. The accuracy in oxygen saturation estimations no longer depend on correct scattering assumptions [23] because scattering parameters are also determined in the process. Moreover, it matches the quantitative performance of wide-field oxygenation imaging using spatially modulated imaging (estimated oxygen saturation values within 5% of the expected values [22]) but avoids additional system complexity. In a preliminary tissue imaging study, the overall tendency in the oxygen saturation values follows the expectations, while the estimated maps of the ratio between the absolute blood concentration and the scattering amplitude and the scattering power remained notably constant and delineate the different organs. These results demonstrate qualitatively the accuracy of the method, but its quantitative validation is subject to further studies including independent measures of the oxygenation values through a different modality. Also, yet to be established is the ability of the recovered scattering power maps beyond organ differentiation, such as whether they provide a distinction between pathological states as those extracted from local reflectance measures. Future research should also focus on the determination of the optimal wavelengths that minimize the error in parameter estimation while accelerating the acquisition.

Funding. Deutsche Forschungsgemeinschaft (DFG); (SFB-824); Bundesministerium für Bildung und Forschung (BMBF) (0315505A); EC FP7 CIG (HIGH-THROUGHPUT TOMO); Spanish MINECO (FIS2013-41802-R).

REFERENCES

1. M. G. Kozberg, B. R. Chen, S. E. DeLeo, M. B. Bouchard, and E. M. Hillman, *Proc. Natl. Acad. Sci. USA* **110**, 4380 (2013).
2. B. P. Joshi, S. J. Miller, C. M. Lee, E. J. Seibel, and T. D. Wang, *Gastroenterology* **143**, 1435 (2012).
3. G. Zonios and A. Dimou, *Opt. Express* **14**, 8661 (2006).
4. N. J. Crane, P. A. Pinto, D. Hale, F. A. Gage, D. Tadaki, A. D. Kirk, I. W. Levin, and E. A. Elster, *BMC Surg.* **8**, 8 (2008).
5. S. Tomatis, M. Carrara, A. Bono, M. Lualdi, G. Tragni, A. Colombo, and R. Marchesini, *Phys. Med. Biol.* **50**, 1675 (2005).
6. M. A. Afromowitz, J. B. Callis, D. M. Heimbach, L. A. DeSoto, and M. K. Norton, *IEEE Trans. Biomed. Eng.* **35**, 842 (1988).
7. D. Mordant, I. Al-Abboud, G. Muyo, A. Gorman, A. Sallam, P. Ritchie, A. R. Harvey, and A. I. McNaught, *Eye* **25**, 309 (2011).
8. L. M. Song, D. G. Adler, J. D. Conway, D. L. Diehl, F. A. Farraye, S. V. Kantsevov, R. Kwon, P. Mamula, B. Rodriguez, R. J. Shah, and W. M. Tierney, *Gastrointest. Endosc.* **67**, 581 (2008).
9. V. Krishnaswamy, P. J. Hoopes, K. S. Samkoe, J. A. O'Hara, T. Hasan, and B. W. Pogue, *J. Biomed. Opt.* **14**, 014004 (2009).
10. A. Cerussi, N. Shah, D. Hsiang, J. Butler, and B. J. Tromber, *J. Biomed. Opt.* **11**, 044005 (2006).
11. A. M. Laughney, V. Krishnaswamy, E. J. Rizzo, M. C. Schwab, R. J. Barth, B. W. Pogue, K. D. Paulsen, and W. A. Wells, *Clin. Cancer Res.* **18**, 6315 (2012).
12. A. Ishimaru, *Wave Propagation and Scattering in Random Media* (Academic, 1978), Vol. 2.
13. J. Ripoll, *Principles of Diffuse Light Propagation: Light Propagation in Tissues with Applications in Biology and Medicine* (World Scientific, 2012).
14. P. Symvoulidis, K. M. Jentoft, P. B. Garcia-Allende, J. Ripoll, and V. Ntziachristos, *Opt. Lett.* **39**, 3919 (2014).
15. T. J. Farrell, M. S. Patterson, and B. A. Wilson, *Med. Phys.* **19**, 879 (1992).
16. R. Aronson and N. Corngold, *J. Opt. Soc. Am. A* **16**, 1066 (1999).
17. R. Aronson, *J. Opt. Soc. Am. A* **12**, 2532 (1995).
18. R. Michels, F. Foschum, and A. Kienle, *Opt. Express* **16**, 5907 (2008).
19. K. Briely-Sab and A. Bjornerud, *Proc. Intl. Sot. Mag. Reson. Med.* **8**, 2025 (2000).
20. S. L. Jacques, *Phys. Med. Biol.* **58**, R37 (2013).
21. H. Bay, A. Ess, T. Tuytelaars, and L. Van Gool, *Comput. Vis. Image Underst.* **110**, 346 (2008).
22. S. Gioux, A. Mazhar, B. T. Lee, A. M. Tobias, D. J. Cuccia, A. Stockdale, R. Oketokoun, Y. Ashitate, E. Kelly, M. Weinmann, N. J. Durr, L. A. Moffitt, A. J. Durkin, B. J. Tromberg, and J. V. Frangioni, *J. Biomed. Opt.* **16**, 086015 (2011).
23. N. T. Clancy, D. Stoyanov, D. R. C. James, A. Di Marco, V. Sauvage, J. Clark, G. Z. Yang, and D. S. Elson, *Biomed. Opt. Express* **3**, 2567 (2012).
24. M. Kohl, U. Lindauer, G. Roy, M. Kuhl, L. Gold, A. Vilringer, and U. Dimagl, *Phys. Med. Biol.* **45**, 3749 (2000).
25. M. B. Bouchard, B. R. Chen, S. A. Burgess, and E. M. Hillman, *Opt. Express* **17**, 15670 (2009).
26. R. Renaud, C. Martin, H. Gurden, and F. Pain, *J. Biomed. Opt.* **17**, 016012 (2012).
27. B. Chance, J. S. Leigh, H. Miyake, D. S. Smith, S. Nioka, R. Greenfeld, M. Finander, K. Kaufmann, W. Levy, and M. Young, *Proc. Natl. Acad. Sci. USA* **85**, 4971 (1988).
28. M. S. Patterson, J. D. Moulton, B. C. Wilson, K. W. Berndt, and J. R. Lakowicz, *Appl. Opt.* **30**, 4474 (1991).
29. D. J. Cuccia, F. Bevilacqua, A. J. Durkin, F. R. Ayers, and B. J. Tromberg, *J. Biomed. Opt.* **14**, 024012 (2009).
30. C. D'Andrea, D. Comelli, A. Pifferi, A. Torricelli, G. Valentini, and R. Cubeddu, *J. Phys. D* **36**, 1675 (2003).